Structural derivation and crystal chemistry of apatites

T. J. White* and Dong ZhiLi

Centre for Advanced Research of Ecomaterials, Institute for Environmental Science and Engineering, Innovation Centre, Nanyang Technological University, Block 2, Unit 237, 18 Nanyang Drive, Singapore 637723

Correspondence e-mail: tjwhite@ntu.edu.sg

The crystal structures of the $[A(1)_2][A(2)_3](BO_4)_3X$ apatites and the related compounds $[A(1)_2][A(2)_3](BO_5)_3X$ and $[A(1)_2][A(2)_3](BO_3)_3X$ are collated and reviewed. The structural aristotype for this family is Mn_5Si_3 ($D8_8$ type, $P6_3/mcm$ symmetry), whose cation array approximates that of all derivatives and from which related structures arise through the systematic insertion of anions into tetrahedral, triangular or linear interstices. The construction of a hierarchy of space-groups leads to three apatite families whose high-symmetry members are $P6_3/m$, $Cmcm$ and $P6_3cm$. Alternatively, systematic crystallographic changes in apatite solid-solution series may be practically described as deviations from regular anion nets, with particular focus on the $O(1)-A(1)-O(2)$ twist angle φ projected on (001) of the $A(1)O_6$ metaprism. For apatites that contain the same A cation, it is shown that φ decreases linearly as a function of increasing average ionic radius of the formula unit. Large deviations from this simple relationship may indicate departures from $P6_3/m$ symmetry or cation ordering. The inclusion of $A(1)O_6$ metaprisms in structure drawings is useful for comparing apatites and condensed-apatites such as $Sr_5(BO_3)_3Br$. The most common symmetry for the 74 chemically distinct $[A(1)_2][A(2)_3](BO_4)_3X$ apatites that were surveyed was $P6_3/m$ (57%), with progressively more complex chemistries adopting $P6_3$ (21%), $P\bar{3}$ (9%), $P\bar{6}$ (4.3%), $P2_1/m$ (4.3%) and $P2_1$ (4.3%). In chemically complex apatites, charge balance is usually maintained through charge-coupled cation substitutions, or through appropriate mixing of monovalent and divalent X anions or X-site vacancies. More rarely, charge compensation is achieved through insertion/removal of oxygen to produce BO_5 square pyramidal units (as in ReO_5) or BO_3 triangular coordination (as in AsO_3). Polysomatism arises through the ordered filling of [001] BO_4 tetrahedral strings to generate the apatite–nasonite family of structures.

1. Introduction

Although the 'apatites' are an industrially important group of materials with applications in catalysis, environmental remediation, bone replacement and ceramic membranes amongst others, to our knowledge there has been no recently published collation of crystallographic data that systematizes the entire range of chemistries and compositions that have been studied to date. In general, the apatite varieties have not been placed in the context of the entire family, with a view to understanding their crystallographic derivation from simpler structures.

The apatite prototype $Ca_5(PO_4)_3F$ structure was first determined by Naray-Szabo (1930) and was confirmed to adopt $P6_3/m$ symmetry. An extensive apatite compilation was

prepared by Wyckoff (1965), who noted that the lack of thorough structure determinations left many unaswered questions about the distribution of metals and oxy-anions. Subsequently, numerous studies of biological, mineralogical and synthetic apatites and apatite-related substances greatly expanded the range of known chemistries. McConnell (1973) summarized the work up to the 1970s and high-lighted the limitations associated with failing to consider the under-lying chemical principles that govern apatite crystallography and the need for precise chemical analyses to properly account for apatite properties. Elliot (1994) updated and expanded the work of McConnell by covering a wider range of apatites, reviewing iso- and altervalent substitutions, and detailing the identification of compounds of lower symmetry. Since then there has been a substantial increase in the number of apatites for which excellent crystallographic data exist. However, the extent of these chemistries, which are convention-ally regarded as conforming to $A_5(BO_4)_3X$, and the relative complexity of the structures have at times obscured either the underlying crystallochemical principles that govern the formation of apatite or the impor-tant systematic changes in crystallography that appear as a function of compositional variation.

In general, structure drawings highlight only the relatively regular BO_4 tetrahedra, while other features are usually grouped as 'irregular' polyhedra. In this paper, we have collated the data of more than 85 chemically distinct apatites for which crystallographic determinations have been completed. These structures are described as anion-stuffed cation arrays of the $D8_8$ alloy type (Wondratschek et al., 1964; O'Keeffe & Hyde, 1985; Vegas & Jansen, 2002) and as deri-vatives of hexagonal anion networks (Povarennykh, 1972). The former approach formalizes the structural hierarchy of apatites with the Mn_5Si_3 structure type at the apex, while the latter proves useful for systematizing topological distortions as a function of average ionic radius. These descriptions also readily accommodate $A_5(BO_3)_3X$ and $A_5(BO_5)_3X$ derivatives and apatite polysomatism. This paper summarizes the current knowledge of apatite structures, particularly with respect to the literature that has appeared since the publication of Elliot's work, and complements the work of Nriagu & Moore (1984) and Brown & Constantz (1994), who deal with phos-phate compounds.
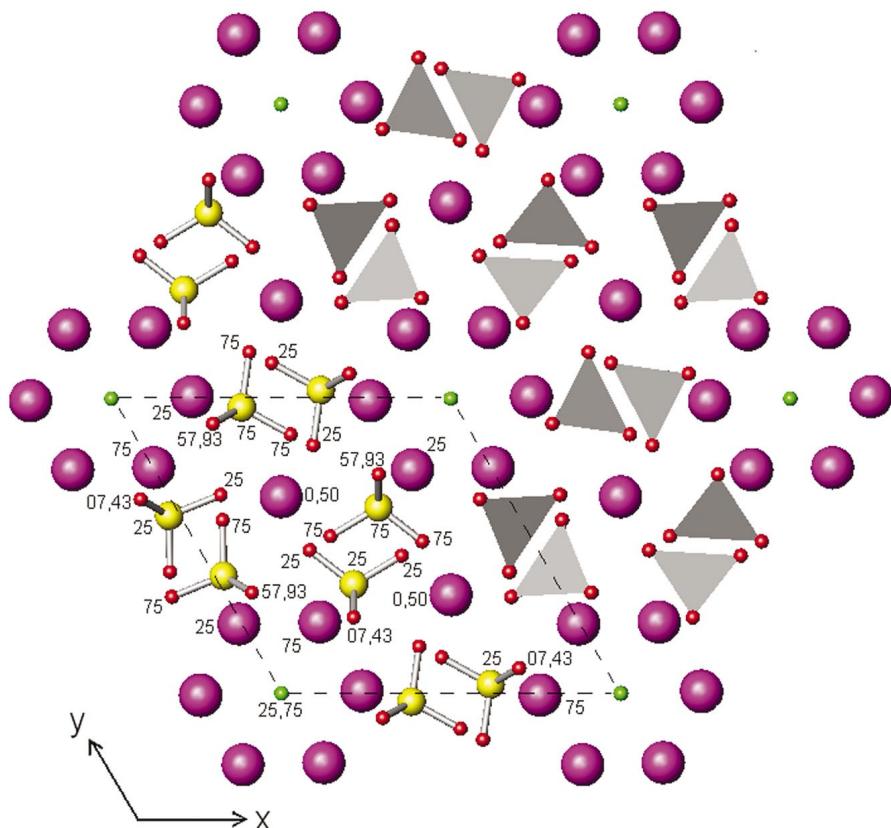

Figure 1
The [001] projection of fluorapatite $Ca_5(PO_4)_3F$ represented in the conventional way with PO_4 units highlighted, as ball and stick or tetrahedral representations, and with the oxygen coordination to the A cations de-emphasized.

2. Structural derivation

2.1. The conventional description

The two most common representations of $P6_3/m$ apatite – in this case $Ca_5(PO_4)_3F$ (Sudarsanan et al., 1972)[1] – are shown in Fig. 1. In general, drawings are projected along [001] and give prominence to the BO_4 tetrahedra, either in ball-and-stick or tetrahedral display. This projection highlights aspects of the symmetry and the regular polyhedra, but usually the coordi-nation of the A cations is not emphasized. Rather, the $A(1)$ ions at the $4f$ position are described as having coordination to nine O atoms (six near and three more distant), while the $A(2)$ ions on the $6h$ position are eight coordinated (to seven O atoms and one F atom). For fluorapatite, the F ion lies at position $2a$ with $z = \frac{1}{4}$, while for larger ions, such as Cl, the $2b$ position with $z = 0$ is occupied. In the latter case, the symmetry can be reduced to monoclinic $P2_1/b$ with the c axis unique and the X ion offset along [001] to statistically occupy the $4e$

---

[1] The refined stoichiometry is $Ca_{4.938}(PO_4)_3F_{0.906}$. It seems likely that many, or perhaps most, of the apatites that are reported as having integral stoichiometry are in fact somewhat non-stoichiometric, particularly with respect to X anions. It is, however, often difficult to determine such compositional variations directly. For this paper, which is concerned primarily with topological arrangements, small deviations from stoichiometry are not directly relevant.

Table 1
Bond lengths (Å) of anion-centred coordination polyhedra.

| Ideal hexagonal net		Chlorapatite		Fluorapatite	
$O(1)-A(1)$	2.300×2	$O(1)-Ca(1)$	2.335×2	$O(1)-Ca(1)$	2.391×2
$O(1)-B$	1.675	$O(1)-P$	1.855	$O(1)-P$	1.534
		$O(1)-Ca(2)$	2.860	$O(1)-Ca(2)$	2.818
$O(2)-A(1)$	2.300×2	$O(2)-Ca(1)$	2.400×2	$O(2)-Ca(1)$	2.451×2
$O(2)-B$	2.901	$O(2)-P$	2.886	$O(2)-P$	3.147
$O(2)-B$	1.592	$O(2)-P$	1.515	$O(2)-P$	1.540
$O(2)-A(2)$	3.138	$O(2)-Ca(2)$	2.335	$O(2)-Ca(2)$	2.384
$O(3)-A(1)$	3.042	$O(3)-Ca(1)$	2.894	$O(3)-Ca(1)$	2.800
$O(3)-B$	2.170	$O(3)-P$	1.592	$O(3)-P$	1.533
$O(3)-A(2)$	2.303	$O(3)-Ca(2)$	2.292	$O(3)-Ca(2)$	2.384
$O(3)-A(2)$	2.365	$O(3)-Ca(2)$	2.455	$O(3)-Ca(2)$	2.395
$X-A(2)$	2.239×6	$Cl-Ca(2)$	2.932×6	$F-Ca(2)$	2.229×3

position to yield an $A(2)O_7Cl$ polyhedron [*e.g.* Bauer & Klee (1993), but see also Kim *et al.* (2000)]. These descriptions, while certainly correct, may not be entirely satisfactory when we seek to relate systematic crystallographic changes as a function of composition or to study structural relationships between apatites. These limitations have been discussed previously by O'Keeffe & Hyde (1985).

2.2. An anion-stuffed $D8_8$ alloy

Alternatively, apatite can be regarded as an anion-stuffed derivative of the Mn_5Si_3 ($D8_8$) alloy type (Wondratschek *et al.*, 1964; O'Keeffe & Hyde, 1985; Nyman & Andersson, 1979; Vegas *et al.*, 1991). Here the A_5B_3 arrangement is emphasized, as in Fig. 2, where the Ca_5P_3 topology of $Ca_5(PO_4)_3F$ is shown.
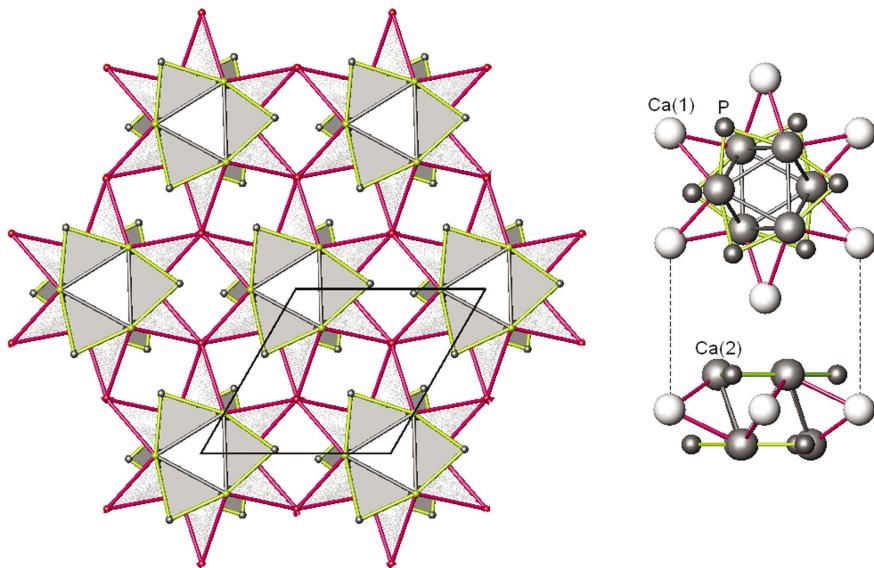
Figure 2
The structure of fluorapatite projected down [001]. We show only the $D8_8$ cation array represented as corner-connected Ca(2) octahedra that are capped on all 12 edges by Ca(1) and P. On the right a single structural $Ca_{12}P_6$ unit is shown projected on [001] in the upper portion and [110] in the lower.
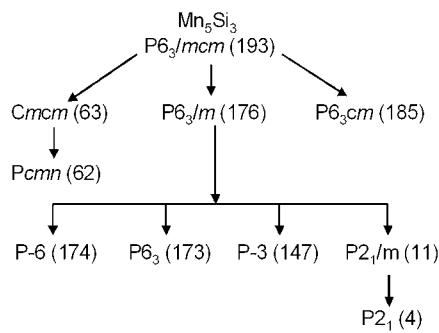
Figure 3
Symmetry relationships for apatite hettotypes that are derived from the Mn_5Si_3 aristotype. [Adapted from Schriewer & Jeitschko (1993).]

This description highlights the regular arrangement of cations and uses a $Ca(2)_6$ octahedron with all edges capped by Ca(1) and P as the fundamental unit. These units are corner-connected in (001) and face sharing along [001]. Anions are then introduced into cavities in the alloy. In fluorapatite, oxygen ions fill tetrahedral [O(1) and O(3)] or trigonal bipyramids [O(2)] while fluorine occupies the triangular interstices between the metals. In chlorapatite the halide moves from triangular to octahedral coordination. A comparison of the bond lengths in these anion-centred polyhedra is summarized in Table 1. Predictably, the oxygen polyhedra are highly distorted since they include $A(1)$, $A(2)$ and B cations, whereas the X-centred triangles and octahedra are regular as they involve $X-A(2)$ bonding only. A similar description has been presented by Schriewer & Jeitschko (1993), who considered the arrangement of the A_5B_3X portion of apatite to be similar to that of the carbide Mo_5Si_3C. The underlying physical basis for the stuffed-alloy model for apatites has recently been considered by Vegas & Jansen (2002), who list the alloy equivalents of 14 varieties.

If the $D8_8$ alloy structure with space group $P6_3/mcm$ is taken as the aristotype – where this terminology is analogous to that adopted to describe perovskites (Lefkowitz *et al.*, 1966; Megaw, 1973) – it follows that anion-stuffed derivatives can adopt maximal non-isomorphic subgroups as shown by the three branches of the hierarchical tree in Fig. 3. Prototypical $A_5(BO_4)_3X$ apatite with $P6_3/m$ symmetry is at the head of the middle branch, and, as discussed below, apatites of lower symmetry ($P6_3$, $P\bar{3}$, $P\bar{6}$, $P2_1/m$, $P2_1$) are numerous. Indeed, it has been suggested by several workers (*e.g.* Huang & Sleight, 1993) that some apatites that are reported to conform to $P6_3/m$ may have lower symmetry, a proposition

that appears to be gaining acceptance as increasing numbers of detailed structure solutions are presented. With respect to the other branches, Aneas *et al.* (1983) and Plaisier *et al.* (1995) have synthesized osmium and rhenium apatites (in which the oxygen coordination of B cations is raised to 5) that have $Pcmn$ and $P6_3cm$ symmetries.

2.3. Hexagonal anion nets

While many crystal structures are regarded as derivatives of near-regular anion packing, this description has not generally been applied to the apatites, although when taken in isolation the anion layers subscribe recognizable, though partially occupied, hexagonal networks. The similarity of the regular anion layers ...**b(ab)a**... for idealized apatite and ...**b(ab′a′b)a**... for (hexagonal) chlorapatite is clear (Fig. 4). The **b** and **b′** layers are differentiated through the twisting of alternate O_3 triangles about [001].

2.3.1. Model I – idealized chlorapatite type. Idealized chlorapatite is constructed by filling trigonal prismatic and tetrahedral interstices in an ordered fashion, such that the $A(1)$ cations are located in the **b** layers and the $A(2)$ and B cations occupy the **a** layers. The atomic coordinates of this derived apatite are given in Table 2, and its structure is illustrated in Fig. 5(*a*). The dominant feature is formed by the $6h$ $A(2)$ cations that occupy $A(2)O_4X_2$ trigonal prism trimers that share common edges along [001]. Filled and empty trigonal prisms alternate along **c**. The $A(1)$ cations form continuous isolated $A(1)O_6$ trigonal prism columns parallel to **c** (Fig. 4a) – for clarity the three more distant O atoms that cap each of the square faces are not indicated. These columns are linked through the BO_4 tetrahedra, which share edges with the $A(2)$ trigonal prisms and corners with the $A(1)$ trigonal prisms. Apatite is not generally represented in this way; however, a notable exception is the short description and associated figure given in Povarennykh (1972), where the A coordination polyhedra are emphasized and described as distorted trigonal prisms.

The similarity of the atomic coordinates and topology of the idealized structure and chlorapatite ($P6_3/m$ symmetry) is obvious, as is the deviation from the perfect hexagonal net (Fig. 5b). In chlorapatite, the largest departure from the ideal position is for the $A(2)$ cation, which is displaced from the centre of the trigonal prism such that it moves closer to O(1)/O(2) and increases its anion coordination from six to eight. This modification allows for the incorporation of larger cations into the structure.

The regular trigonal prisms of the $A(1)$ cations are converted into metaprisms through the twisting of oxygen triangles, as described above, to generate a polyhedron that is intermediate between a trigonal prism and an octahedron (O'Keeffe & Hyde, 1996). This twist angle φ, which is the (001) projection of O(1)−$A(1)$−O(2), is equal to 19.1° (Fig. 6). The reduced volume of the metaprism permits the accommodation of relatively smaller cations.

2.3.2. Model II – idealized fluorapatite type. The ideal fluorapatite model retains $A(1)O_6$ and BO_4 polyhedra iden-

Table 2
Crystal data for idealized apatite compared with crystal data for chlorapatite and fluorapatite.

Idealized hexagonal net, model I with $A(2)$ trigonal prisms, $a \sim 9.5$ Å, $c \sim 6.9$ Å

Chlorapatite (Hendricks *et al.*, 1932), $a = 9.532$ Å, $c = 6.850$ Å

$A(1)$	$4f$	1/3	2/3	0	$Ca(1)$	$4f$	1/3	2/3	0.000
$A(2)$	$6h$	0.1667 (1/6)	0.042 (1/24)	1/4	$Ca(2)$	$6h$	1/4	0	1/4
B	$6h$	0.4231 (11/26)	0.3846 (5/13)	1/4	P	$6h$	0.417	0.361	1/4
O1	$6h$	0.3847 (5/13)	0.5385 (7/13)	1/4	O1	$6h$	1/3	1/2	1/4
O2	$6h$	0.6153 (8/13)	0.4615 (6/13)	1/4	O2	$6h$	0.600	0.467	1/4
O3	$12i$	0.3077 (4/13)	0.2308 (3/13)	0	O3	$12i$	1/3	1/4	0.064
X	$2b$	0	0	0	Cl	$2b$	0	0	0

Idealized hexagonal net, model II with $A(2)$ octahedra, $a \sim 9.5$ Å, $c \sim 6.9$ Å

Fluorapatite (Sudarsanan *et al.*, 1972) $a = 9.363$ (2) Å, $c = 6.878$ (2) Å

$A(1)$	$4f$	1/3	2/3	0	$Ca(1)$	$4f$	1/3	2/3	0.0012
$A(2)$	$6h$	0.1923 (5/26)	0.0769 (1/13)	1/4	$Ca(2)$	$6h$	0.2413	0.0071	1/4
B	$6h$	0.4231 (11/26)	0.3846 (5/13)	1/4	P	$6h$	0.3982	0.3689	1/4
O1	$6h$	0.3847 (5/13)	0.5385 (7/13)	1/4	O1	$6h$	0.3268	0.4850	1/4
O2	$6h$	0.6153 (8/13)	0.4615 (6/13)	1/4	O2	$6h$	0.5881	0.4668	1/4
O3	$12i$	0.3077 (4/13)	0.2308 (3/13)	0	O3	$12i$	0.3415	0.2569	0.0704
X	$2b$	0	0	1/4	F	$2a$	0	0	1/4

Idealized hexagonal net, model III with $A(1)$ octahedra, $a \sim 9.5$ Å, $c \sim 5.4$ Å

$A(1)$	$4f$	1/3	2/3	0
$A(2)$	$6h$	0.1667 (1/6)	0.3333 (1/3)	1/4
B	$6h$	0.3333 (1/3)	0.3333 (1/3)	1/4
O1	$6h$	0.3333 (1/3)	0.5000 (1/2)	1/4
O2	$6h$	0.6667 (2/3)	0.5000 (1/2)	1/4
O3	$12i$	0.1667 (1/6)	0.1667 (1/6)	0
X	$2b$	0	0	0

tical to those of the chlorapatite model; however, because the X anions are displaced by $z/4$, the coordination sphere of $A(2)$ changes to octahedral $A(2)O_5X$ (Fig. 7a, Table 2). These octahedra, which are corner-connected to each other and to the $A(1)O_6$ trigonal prisms, are cation-centred on the **b** anion nets, and form groupings of three, which are joined at a common X atom at one of their apices. The $A(2)$ octahedra parallel to (001) edge-share with the BO_4 tetrahedra. This description of apatite was put forward by Alberius-Henning, Landa-Canovas *et al.* (1999), who regarded the $A(2)O_5X$ octahedral arrangement as NaCl-like. For the real fluorapatite structure the $A(1)$ metaprismatic twist angle $\varphi = 23.3°$ (Figs. 6 and 7b).

2.3.3. Model III – idealized glaserite type. In models I and II the $A(1)O_6$ trigonal prismatic coordination was retained,

albeit somewhat elongated along [001]. However, in real chlor- and fluorapatite, the twisting converted these polyhedra to metaprisms. The maximum possible twist angle φ is 60°, in which case $A(1)O_6$ coordination is octahedral (Fig. 6), if collapse is invoked along [001] to maintain edges of equal

length, or elongated octahedral otherwise. The fractional coordinates of the atoms in this arrangement, which can be described as a double h.c.p. structure, are given in Table 2. While no real structure that adopts this arrangement could be identified, layers of this type are found in the glaserite-type
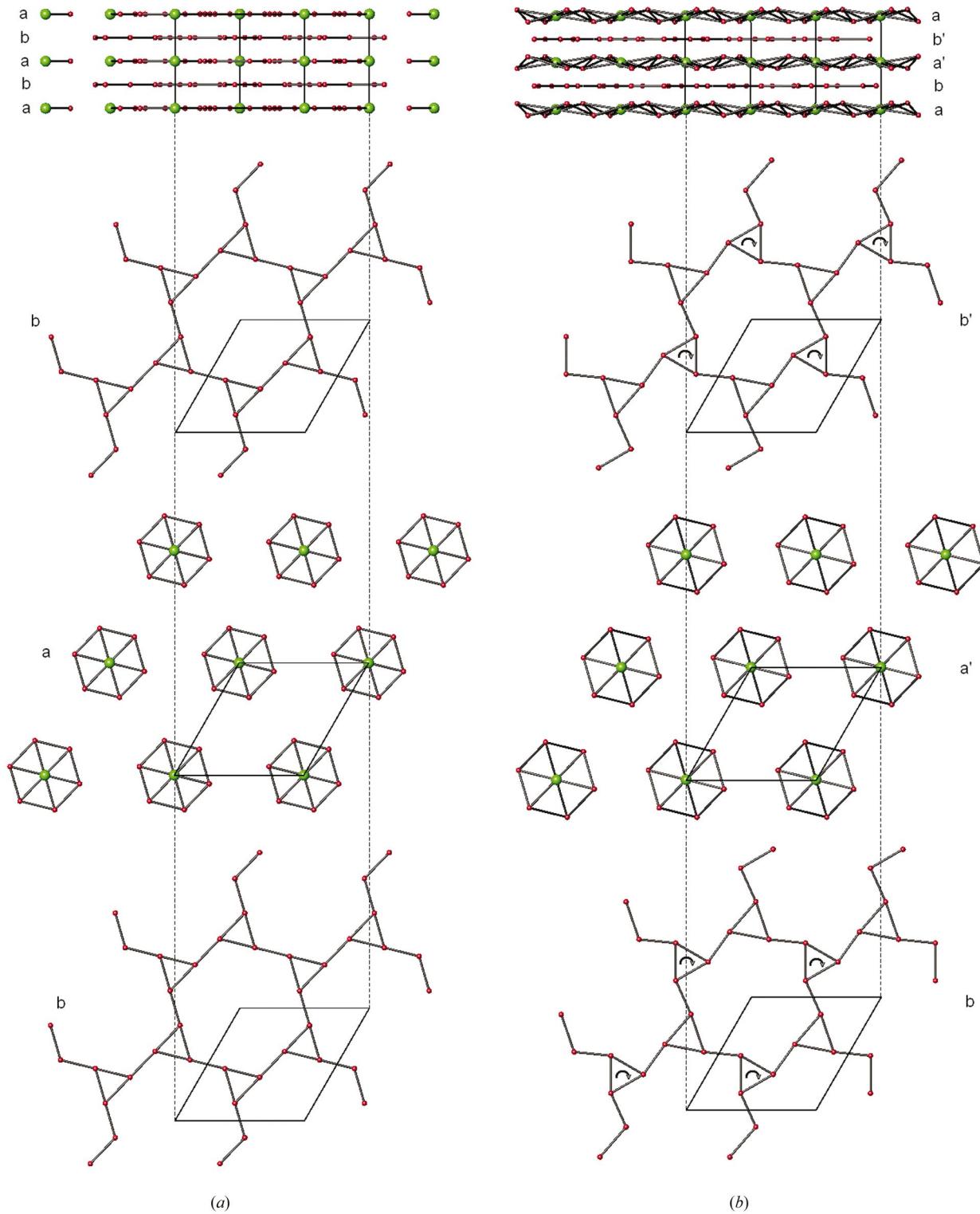

(a)   (b)

Figure 4
The anion arrangement in (a) idealized chlorapatite and (b) the real chlorapatite structure. The upper portion shows the [110] projection and emphasizes the stacking sequence using the conventional ...**b(ab)a**... notation. In real chlorapatite, anion displacements lead to a doubling of the [001] crystallographic repeat and hence to the sequence ...**b(ab′a′b)a**.... In the lower portion three (001) anion slices are drawn. The anion layers are evidently not fully occupied although their derivation from a triangular network is clear.

structure. Indeed the formal relationship between glaserite [typified by $P\bar{3}$ $K_3Sc(PO_4)_2$] and apatite has been discussed by Wondratschek (1963).
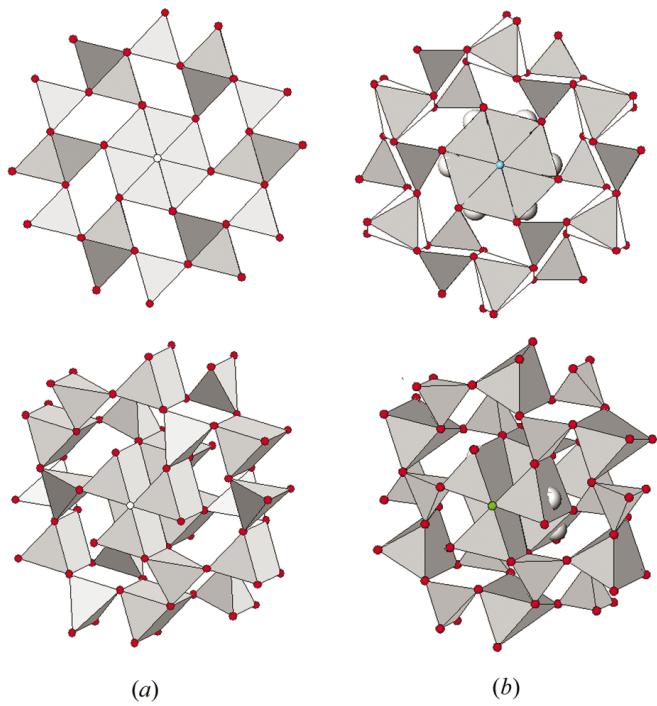

Figure 5
Arrangement of cation-centred polyhedra in (*a*) model I, which approximates the arrangement in chlorapatite, and (*b*) the refined structure of chlorapatite. In the upper part the projection along [001] is shown, while $A(1)O_6$, $A(2)O_4X_2$ and BO_4 connectivity is emphasized in the lower clinographic projections. Note that the statistical occupancy of chlorine is not considered in this representation.
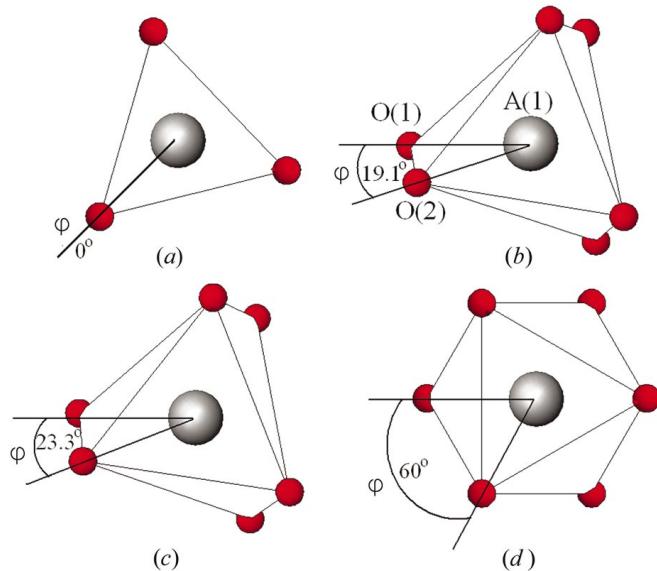

Figure 6
Twist angles of $A(1)O_6$ polyhedra in (*a*) models I and II, (*b*) chlorapatite, (*c*) fluorapatite, and (*d*) model III (as found in glaserite).

3. Apatites with BO_4 tetrahedra

A compilation of 77 distinct $A_5(BO_4)_3X$ compounds for which complete crystallographic data exist is presented in Table 3. It is recognized that the occurrence of chemical analogues is more widespread (*e.g.* Cockbain, 1968). However, for this analysis single-crystal determinations or powder refinements are essential. Similarly, intermediate members of solid-solution series were not included, except where information for the chemical endmembers was unavailable or complex chemistries led to lower symmetries.

While $P6_3/m$ is dominant (57% of the total), apatites lower in the hierarchical tree are not uncommon, especially $P6_3$ (21%) and $P\bar{3}$ (9%). Lower symmetries result from an increase in chemical complexity, as a greater number of acceptor sites (seven in $P6_3/m$ and 18 in $P2_1/m$) are required to accommodate the different bonding requirements of the A and B cations (Table 4). Note that apatites that adopt $P2_1/b$ do so because statistical occupation of the $4e$ site by the X anion (Cl^- or OH^-) is required – the rest of the structure maintains $P6_3/m$. Therefore, monoclinic apatites such as $Ca_{4.95}(PO_4)_{2.99}Cl_{0.92}$ (Ikoma *et al.*, 1999) are not strictly accommodated through direct derivation from the $D8_8$ aristotype. Rather they can be considered as interpenetrating lattices of commensurate structure (that based on $D8_8$) and (in)commensurate structure of resulting X-anion–X-vacancy ordering.
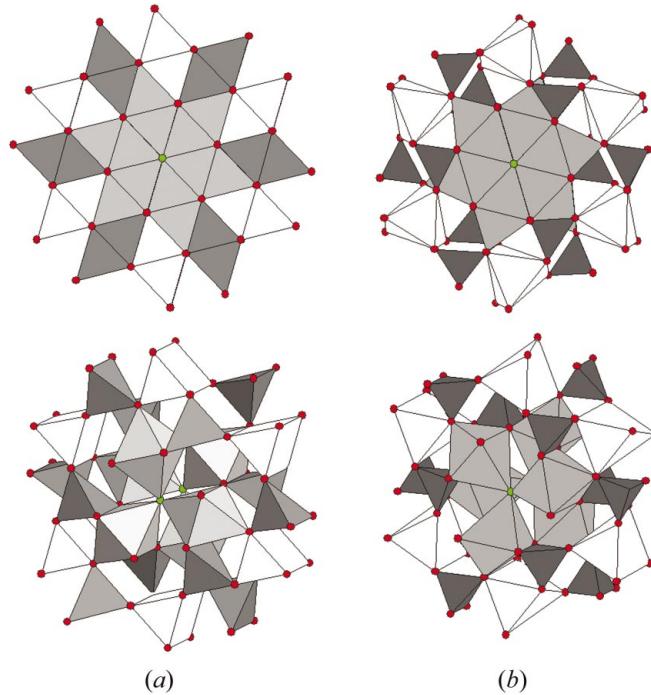

Figure 7
Arrangement of cation-centred polyhedra in (*a*) model II, which approximates the arrangement in fluorapatite, and (*b*) the refined structure of fluorapatite. In the upper part the projection along [001] is shown, while $A(1)O_6$, $A(2)O_5X$ and BO_4 connectivity is emphasized in the lower clinographic projections.

Table 3
$[A(1)_2][A(2)_3](BO_4)_3X$ apatites.

Space group/ mineral name	Composition	Unit-cell parameters (Å)	Reference
$P6_3/m$ (176)			
	$Na_{6.35}Ca_{3.65}(SO_4)_6F_{1.65}$	$a = 9.4364$ (21), $c = 6.9186$ (16)	Piotrowski, Kahlenberg & Fischer (2002)
	$Na_{6.39}Ca_{3.61}(SO_4)_6Cl_{1.61}$	$a = 9.5423$ (1), $c = 6.8429$ (1)	Piotrowski, Kahlenberg & Fischer (2002)
Carocolite (high)	$Na_3Pb_2(SO_4)_3Cl$	$a = 9.810$ (20), $c = 7.140$ (20)	Schneider (1967)
	$Na_3Pb_2(BeF_4)_3F$	$a = 9.531$ (3), $c = 7.028$ (2)	Engel & Fischer (1990)
	$Na_2Ca_6Sm_2(PO_4)_6F_2$	$a = 9.3895$ (3), $c = 6.8950$ (4)	Toumi et al. (2000)
Fluroapatite	$Ca_5(PO_4)_3F$	$a = 9.363$ (2), $c = 6.878$ (2)	Sudarsanan et al. (1972)
Chlorapatite	$Ca_5(PO_4)_3Cl$	$a = 9.5902$ (6), $c = 6.7666$ (2)	Kim et al. (2000); Hendricks et al. (1932)
	$Ca_5(PO_4)_3Br$	$a = 9.761$ (1), $c = 6.739$ (1)	Elliot et al. (1981); Kim et al. (2000)
	$Ca_5(PO_4)_3OH$	$a = 9.4302$ (5), $c = 6.8911$ (2)	Kim et al. (2000; Hughes et al. (1989)
	$Ca_{15}(PO_4)_9IO$†	$a = 9.567$, $c = 20.758$	Alberius-Henning, Lidin & Petrícek (1999)
	$Ca_5(CrO_4)_3OH$	$a = 9.683$, $c = 7.010$	Wilhelmi & Jonsson (1965)
Tourneaurite	$Ca_5(AsO_4)_3Cl$	$a = 10.076$ (1), $c = 6.807$ (1)	Wardojo & Hwu (1996)
Hedyphane	$Ca_2Pb_3(AsO_4)_3Cl$	$a = 10.140$ (3), $c = 7.185$ (4)	Rouse et al. (1984)
	$Sr_5(PO_4)_3Cl$	$a = 9.877$ (0), $c = 7.189$ (0)	Nötzold et al. (1994)
	$Sr_5(PO_4)_3Br$	$a = 9.964$ (0), $c = 7.207$ (0)	Nötzold & Wulff (1998)
	$Sr_5(PO_4)_3OH$	$a = 9.745$ (1), $c = 7.265$ (1)	Sudarsanan & Young (1972)
	$(Sr_{4.909}Nd_{0.061})(V_{0.972}O_4)_3F_{0.98}$	$a = 10.0081$ (1), $c = 7.434$ (1)	Corker et al. (1995)
	$Sr_5(VO_4)_3(Cu_{0.896}O_{0.95})$	$a = 10.126$ (1), $c = 7.415$ (1)	Carrillo-Cabrera & von Schnering (1999)
	$Cd_{4.92}(PO_4)_3Cl_{0.907}$	$a = 9.633$ (4), $c = 6.484$ (4)	Sudarsanan et al. (1977); Wilson et al. (1977)
	$Cd_5(PO_4)_3Cl$	$a = 9.625$ (4), $c = 6.504$ (2)	Ivanov et al. (1976); Sudarasanan et al. (1973)
	$Cd_{4.82}(PO_4)_3Br_{1.52}$	$a = 9.733$ (1), $c = 6.468$ (1)	Sudarsanan et al. (1977); Wilson et al. (1977)
	$Cd_5(PO_4)_3OH$	$a = 9.335$ (2), $c = 6.664$ (3)	Hata et al. (1978)
	$Cd_{4.92}(AsO_4)_3Br_{1.52}$	$a = 10.100$ (1), $c = 6.519$ (1)	Sudarsanan et al. (1977); Wilson et al. (1977)
	$Cd_{4.64}(VO_4)_3I_{1.39}$	$a = 10.307$ (1), $c = 6.496$ (1)	Sudarsanan et al. (1977); Wilson et al. (1977)
	$Cd_{4.86}(VO_4)_3Br_{1.41}$	$a = 10.173$ (2), $c = 6.532$ (1)	Sudarsanan et al. (1977); Wilson et al. (1977)
	$Ba_5(PO_4)_3F$	$a = 10.153$ (2), $c = 7.733$ (1)	Mathew et al. (1979)
	$Ba_5(PO_4)_3Cl$	$a = 10.284$ (2), $c = 7.651$ (3)	Hata et al. (1979)
	$Ba_5(AsO_4)_2SO_4S$	$a = 10.526$ (5), $c = 7.737$ (1)	Schiff-Francois et al. (1979)
	$Ba_5(MnO_4)_3F$	$a = 10.3437$, $c = 7.8639$	Dardenne et al. (1999)
	$Ba_5(MnO_4)_3Cl$	$a = 10.469$ (1), $c = 7.760$ (1)	Reinen et al. (1986)
	$Pb_5(PO_4)_3F$	$a = 9.760$ (8), $c = 7.300$ (8)	Belokoneva et al. (1982); Kim et al. (2000)
Pyromorphite	$Pb_5(PO_4)_3Cl$	$a = 9.998$ (1), $c = 7.344$ (1),	Dai & Hughes (1989); Kim et al. (2000)
	$Pb_5(PO_4)_3Br$	$a = 10.0618$ (3), $c = 7.3592$ (1)	Kim et al. (2000)
	$Pb_5(PO_4)_3OH$	$a = 9.866$ (3), $c = 7.426$ (2)	Bruecker et al. (1995); Kim et al. (1997, 2000); Barinova et al. (1998)
Vanadinite	$Pb_5(VO_4)_3Cl$	$a = 10.317$ (3), $c = 7.338$ (3)	Dai & Hughes (1989)
	$Pb_{9.85}(VO_4)_6I_{1.7}$	$a = 10.442$ (5), $c = 7.467$ (3)	Audubert et al. (1999)
Mimetite	$Pb_5(AsO_4)_3Cl$	$a = 10.211$ (1), $c = 7.418$ (4)	Calos & Kennard (1990)
	$Pb_5(GeO_4)(VO_4)_2$	$a = 10.097$ (3), $c = 7.396$ (2)	Ivanov & Zavodnik (1989); Ivanov (1990)
	$Pb_5(SO_4)(GeO_4)_2$	$a = 10.058$ (4), $c = 7.416$ (1)	Engel & Deppisch (1988)
	$Pb_5(CrO_4)(GeO_4)_2$	$a = 10.105$ (3), $c = 7.428$ (2)	Engel & Deppisch (1988)
	$Pb_3(PO_4)_2$	$a = 9.826$ (4), $c = 7.357$ (3)	Hata et al. (1980)
	$Pb_4Na(VO_4)_3$	$a = 10.059$ (3), $c = 7.330$ (1)	Sirotinkin et al. (1989)
	$Pb_8K_2(PO_4)_6$	$a = 9.827$ (1), $c = 7.304$ (5)	Mathew et al. (1980)
	$Mn_5(PO_4)_3Cl_{0.9}(OH)_{0.1}$	$a = 9.532$ (1), $c = 6.199$ (1)	Engel et al. (1975)
	$Nd_4Mn(SiO_4)_3O$	$a = 9.499$ (1), $c = 6.944$ (2)	Kluever & Mueller-Buschbaum (1995)
	$NaY_9(SiO_4)_6O_2$	$a = 9.332$ (2), $c = 6.759$ (1)	Gunawardane et al. (1982)
	$La_9Na(GeO_4)_6O_2$	$a = 9.883$ (2), $c = 7.267$ (3)	Takahashi et al. (1998)
	$La_{10}(Si_{3.96}B_{1.98}O_4)_6O_2$	$a = 9.5587$ (2), $c = 7.2171$ (2)	Mazza et al. (2000)
	$La_3Nd_{11}(SiO_4)_9O_3$†	$a = 9.638$ (2), $c = 21.350$ (8)	Malinovskii et al. (1990)
Britholite	$(Ce_{0.4}Ca_{0.35}Sr_{0.25})_2(Ce_{0.86}Ca_{0.14})_3(SiO_4)_3(O_{0.5}F_{0.38})$	$a = 9.638$ (1), $c = 7.081$ (1)	Genkina et al. (1991)

Table 3 (continued)

Space group/ mineral name	Composition	Unit-cell parameters (Å)	Reference
$P6_3$ (173)			
	$K_3Sn_2(SO_4)_3Cl$	$a = 10.230$ (20), $c = 7.560$ (20)	Howie *et al.* (1973); Donaldson & Grimes (1984)
	$K_3Sn_2(SO_4)_3Br$	$a = 10.280$ (20), $c = 7.570$ (20)	Howie *et al.* (1973); Donaldson & Grimes (1984)
	$KNd_9(SiO_4)_6O_2$	$a = 9.576$ (2), $c = 7.009$ (2)	Pushcharovskii *et al.* (1978)
	$Ca_{10}(PO_4)_6S$	$a = 9.455$ (0), $c = 8.840$ (0)	Sutich *et al.* (1986)
	$Ca_4Bi(VO_4)_3O$	$a = 9.819$ (2), $c = 7.033$ (2)	Huang & Sleight (1993)
	$Sr_{7.3}Ca_{2.7}(PO_4)_6F_2$	$a = 9.865$ (8), $c = 7.115$ (3)	Pushcharovskii *et al.* (1987); Klevtsova (1964)
	$Sr_5(CrO_4)_3Cl$	$a = 10.125$, $c = 7.328$	Mueller-Buschbaum & Sander (1978)
	$Cd_5(PO_4)_3OH$†	$a = 16.199$ (0), $c = 6.648$ (0)	Hata & Marumo (1983)
	$Ba_5(PO_4)_3OH$	$a = 10.190$ (1), $c = 7.721$ (2)	Bondareva & Malinovskii (1986)
	$Ba_5(CrO_4)_3OH$	$a = 10.428$, $c = 7.890$	Mattausch & Mueller-Buschbaum (1973)
	$Ba_5[(Ge,C)(O,OH)_4)]_3[(CO_3(OH)]_{1.5}(OH)$	$a = 10.207$ (3), $c = 7.734$ (2)	Malinovskii *et al.* (1975)
	$La_6Ca_{3.5}(SiO_4)_6(H_2O)F$	$a = 9.664$ (3), $c = 7.090$ (1)	Kalsbeek *et al.* (1990)
	$Na_{0.97}Ca_{1.40}La_{2.20}Ce_{3.69}Pr_{0.32}Nd_{0.80}[(Si_{5.69}P_{0.31})_4]_6(OH,F)$	$a = 9.664$ (3), $c = 7.090$ (1)	Kalsbeek *et al.* (1990)
	$Sm_{10}(SiO_4)_6N_2$	$a = 9.517$ (6), $c = 6.981$ (4)	Gaude *et al.* (1975)
	$(Sm_8Cr_2)(SiO_4)_6N_2$	$a = 9.469$ (5), $c = 6.890$ (4)	Maunaye *et al.* (1976)
$P\bar{3}$ (147)			
	$Ca_{9.93}(P_{5.84}B_{0.16}O_4)_6(B_{0.67}O_{1.79})$	$a = 9.456$ (1), $c = 6.905$ (1)	Ito *et al.* (1988)
	$Sr_{9.402}Na_{0.209}(PO_4)_6B_{0.996}$	$a = 9.734$ (4), $c = 7.279$ (2)	Calvo *et al.* (1982)
	$Ba_4Nd_3Na_3(PO_4)_6F_2$	$a = 9.786$ (2), $c = 7.281$ (1)	Mathew *et al.* (1979)
Belovite	$Na_{0.5}Ca_{0.3}Ce_{1.00}Sr_{2.95}(PO_4)_3OH$	$a = 9.692$ (3), $c = 7.201$ (1)	Nadezhina *et al.* (1987)
	$Na_{0.981}La_{0.999}Sr_{2.754}Ba_{0.12}Ca_{0.06}(PO_4)_3OH$	$a = 9.664$ (0), $c = 7.182$ (0)	Kabalov *et al.* (1997)
	$Na_2Ca_2Sr_6(PO_4)_6(OH)_2$	$a = 9.620$, $c = 7.120$	Klevtsova & Borisov (1964)
$P\bar{6}$ (174)			
Cesanite	$Na_{6.9}Ca_{3.1}(SO_4)_6OH_{1.1}$	$a = 9.4434$ (13), $c = 6.8855$ (14)	Piotrowski *et al.* (2002)
	$Ca_{10}(PO_4)_6O$	$a = 9.432$, $c = 6.881$	Alberius-Henning, Landa-Canovas *et al.* (1999)
	$Ba_3LaNa(PO_4)_3F$	$a = 9.939$ (0), $c = 7.442$ (1)	Mathew *et al.* (1979)
$P2_1/m$ (11)			
Hydroxyellestad- tite	$Ca_{10}(SiO_4)_3(SO_4)_3[F_{0.16}Cl_{0.48}(OH)_{1.36}]$	$a = 9.476$ (2), $b = 9.508$ (2), $c = 6.919$ (1), $\gamma = 119.5°$	Sudarsanan (1980); Hughes & Drexler (1991)
Fermorite	$(Ca_{8.40}Sr_{1.61})(AsO_4)_{2.58}(PO_4)_{3.42}F_{0.69}(OH)_{1.31}$	$a = 9.594$ (2), $b = 9.597$ (2), $c = 6.975$ (2), $\gamma = 120.0$ (0)°	Hughes & Drexler (1991)
Carocolite (low)	$Na_3Pb_2(SO_4)_3Cl$†	$a = 19.620$, $b = 9.810$, $c = 7.140$, $\gamma = 120°$	Schneider (1969)
$P2_1/b$ (14)			
	$Ca_5(PO_4)_3OH$	$a = 9.421$ (1), $b = 18.843$ (2), $c = 6.881$ (1), $\gamma = 120.0$ (1)°	Elliot *et al.* (1973)
	$Ca_{4.95}(PO_4)_{2.99}Cl_{0.92}$	$a = 9.426$ (3), $b = 18.856$ (5), $c = 6.887$ (1), $\gamma = 119.97$ (1)°	Ikoma *et al.* (1999)
	$Ca_{9.97}(PO_4)_3Cl_{1.94}$†	$a = 9.632$ (7), $b = 19.226$ (20), $c = 6.776$ (5), $\gamma = 119.9$ (1)°	Bauer & Klee (1993); Mackie *et al.* (1972)
Clinomimetite	$Pb_5(AsO_4)_3Cl$†	$a = 10.189$ (3), $b = 20.372$ (6), $c = 7.456$ (6), $\gamma = 119.0$ (0)°	Dai *et al.* (1991)
$P2_1$ (4)			
Ellestadite (low)	$Ca_{10}(Si_{3.14}S_{2.94}C_{0.08}P_{0.02})O_{24}[(OH)_{1.12}Cl_{0.316}F_{0.05}]$	$a = 9.526$ (2), $b = 9.506$ (4), $c = 6.922$ (1), $\gamma = 120.0$ (0)°	Organova *et al.* (1994)
Britholite	$(Na_{1.46}La_{8.55})(SiO_4)_6(F_{0.9}O_{0.11})$	$a = 9.678$ (1), $b = 9.682$ (3), $c = 7.1363$ (1), $\gamma = 120.0$ (0)°	Hughes *et al.* (1992)
Britholite (Ce)	$(Ca_{2.15}Ce_{2.85})(SiO_4)_3[F_{0.5}(OH)_{0.5}]$	$a = 9.580$ (5), $b = 9.590$ (4), $c = 6.980$ (3), $\gamma = 120.1$ (0)°	Noe *et al.* (1993)

† Superstructure.

3.1. *A*(1) metaprism twist angle

The metaprism twist angle φ is, not surprisingly, sensitive to apatite composition – the smallest ($\varphi = 5.2°$) is found for $Ca_2Pb_3(AsO_4)_3Cl$, while the largest ($\varphi = 26.7°$) has been observed for $Pb_5(PO_4)_3OH$ (Fig. 8). For $P6_3/m$ apatites φ can be calculated for any individual metaprism from the fractional coordinates of $A(1)$, O(1) and O(2) *via* the general expression

Table 4
Atom acceptor sites in apatites that adopt different space groups.

| Site types | Space group | | | | | | | | | |
| | $P6_3/m$ (176) | | $P6_3$ (173) | | $P\bar{3}$ (147) | | $P\bar{6}$ (174) | | $P2_1/m$ (11) | |
	Wyckoff number	Number of site types	Wyckoff number	Number of site types	Wyckoff number	Number of site types	Wyckoff number	Number of site types	Wyckoff number	Number of site types
Large A cations	$6h$	1	$6c$	1	$6g$	1	$3k, 3j$	2	$2a, 2e \times 2$	3
Small A cation	$4f$	1	$2b \times 2$	2	$2d \times 2$	2	$2i, 2h$	2	$4f$	1
B cations	$6h$	1	$6c$	1	$6g$	1	$3k, 3j$	2	$2e \times 3$	3
Total number of cation acceptor sites		3		4		4		6		7
Oxygen anions	$6h \times 2, 12i$	3	$6c \times 4$	4	$6g \times 4$	4	$3k \times 2, 3j \times 2, 6l \times 2$	6	$2e \times 6, 4f \times 3$	9
X anions	$2a$ or $2b$ or $4e$	1	$2a$	1	$1a, 1b$	2	$1a, 1b$ or $2g$	1/2	$2a$ or $2e$	2
Total number of anion acceptor sites		4		5		6		7/8		11
Examples of cation occupancy	$[Ca_6][Ca_4][P_6]$		$[K_6][K_2Sn_2][S_6]$		$[Ba_4Nd_1Na_1][Nd_2Na_2][P_6]$		$[Ba_5La_1][La_1Na_{1.3}Ba_{1.7}][P_6]$		$[Ca_6][Ca_4][Si_3S_3]$	
$[A_6][A_4][B_6]$-$[O_{24}][X_2]$	$Ca_{10}(PO_4)_6F_2$		$K_6Sn_4(SO_4)_6Cl_2$		$Ba_4Nd_3Na_3(PO_4)_6F_2$		$Ba_{6.7}La_2Na_{1.3}(PO_4)_6F_2$		$Ca_{10}(SiO_4)_3(SO_4)_3$ $[F_{0.16}Cl_{0.48}(OH)_{1.36}]$	

$$\cos \varphi = \left[(G_3 - G_1)^2 + (H_3 - H_1)^2 + (G_1 - G_2)^2 \right.$$
$$\left. + (H_1 - H_2)^2 - (G_2 - G_3)^2 - (H_2 - H_3)^2 \right]$$
$$/ \left(2 \left\{ \left[(G_3 - G_1)^2 + (H_3 - H_1)^2 \right] \right. \right.$$
$$\left. \left. \times \left[(G_1 - G_2)^2 + (H_1 - H_2)^2 \right] \right\}^{1/2} \right),$$

where

$$G_1 = 0.866 x_{A1}, \quad H_1 = y_{A1} - 0.5 x_{A1},$$

$$G_2 = 0.866 x_{O1}, \quad H_2 = y_{O1} - 0.5 x_{O1},$$

$$G_3 = 0.866 x_{O2}, \quad H_3 = y_{O2} - 0.5 x_{O2}.$$

When φ is calculated for a range of apatites, it is observed to vary inversely with average crystal radii and unit-cell volume (Table 5). In fact, for those $P6_3/m$ apatites with the same A cation (*e.g.* calcium or cadmium), the relationship is very nearly linear (Fig. 9), regardless of whether substitution is made on the B or X sites. In other words, for apatites with smaller average crystal radii, the structure must collapse further to satisfy shorter bond-length requirements, and this fact is reflected in larger φ values, which lead to shorter $A(1)$—O distances. If $A(1)O_6$ twisting is considered to be the pivotal structural feature, then the collapse towards octahedral bonding will also accommodate the shortening of the cell edges and a general reduction of $A(2)$—O—X bond lengths. [A detailed consideration of the geometry of metaprism twisting is given in Dong & White (2003).] In contrast the BO_4 tetrahedra will essentially remain invariant. Therefore, the metaprism twist angle φ is a useful qualitative – and in some

cases quantitative – predictor of apatite distortion from ideal h.c.p. packing. Indeed, for all the apatites in Table 5 only two compositions were exceptional. $Ba_5(MnO_4)_3Cl$ (Reinen *et al.*, 1986) and $Pb_5(PO_4)_3OH$ (Bruecker *et al.*, 1995) have φ values of 22.3° and 26.7°, respectively. These appear anomalously high compared with the average crystal radii and bond angle (Table 5). Possible explanations may be the adoption of lower symmetry, the distortion of the MnO_4 tetrahedra or A-site non-stoichiometry for the Pb compound.

3.2. X-site non-stoichiometry

It has long been understood that larger X anions (Cl, Br, I) may be displaced away from their $2a$ and $2b$ special positions, especially if the $A(2)$ sites are occupied by smaller cations, and that a portion of the sites may be vacant. Substantial quantitative treatments of the phenomena have been undertaken by several workers (*e.g.* Kim *et al.*, 2000; Hashimoto & Matsumoto, 1998; Hata *et al.*, 1979; Mackie *et al.*, 1972). While the location of the anions over available sites is generally assumed to be statistical, it has now been demonstrated that cadmium phosphate bromate and cadmium vanadate iodate exhibit incommensurate ordering of X anions and vacancies (Christy *et al.*, 2001). For lead-rich apatites the X site may be completely vacant, as in $Pb_3(PO_4)_2$, $Pb_4Na(VO_4)_3$ and $Pb_8K_2(PO_4)_6$. It is reasonable to assume that the stereochemically active lone pair of Pb^{2+}, which occupies a volume close to that of oxygen, allows such compounds to be stable (Mathew *et al.*, 1980). Stoichiometrically similar non-lead-bearing compounds [*e.g.* $Cd_5(PO_4)_2GeO_4$], which do not have the benefit of lone-pair stabilization, adopt the carnotite

Table 5
Twist angle (φ), average crystal radius per unit-cell content and unit-cell volume.

Composition	Metaprism angle (°)	Average crystal radius (Å)†	Volume (Å³)
$Ca_{10}(PO_4)_6F_2$	23.3	1.143	522.6
$Ca_{10}(PO_4)_6OH_2$	23.2	1.146	530.3
$Ca_{10}(PO_4)_6Cl_2$	19.1	1.166	537.6
$Ca_{10}(CrO_4)_6OH_2$	17.8	1.171	569.2
$Ca_{10}(PO_4)_6Br_2$	16.3	1.173	556.1
$Ca_{10}(AsO_4)_6Cl_2$	13.0	1.189	598.5
$Ca_4Pb_6(AsO_4)_6Cl_2$	5.2	1.214	639.8
$Cd_{10}(PO_4)_6OH_2$	25.8	1.139	502.9
$Cd_{10}(PO_4)_6Cl_2$	19.5	1.158	521.1
$Cd_{10}(PO_4)_6Br_2$	16.0	1.165	530.6
$Cd_{10}(AsO_4)_6Br_2$	11.6	1.189	575.9
$Cd_{10}(VO_4)_6Br_2$	8.8	1.192	585.4
$Cd_{10}(VO_4)_6I_2$	8.4	1.203	597.6
$Sr_{10}(PO_4)_6OH_2$	23.0	1.183	597.5
$Sr_{10}(PO_4)_6Cl_2$	21.1	1.203	606.6
$Sr_{10}(PO_4)_6Br_2$	19.6	1.210	619.7
$Pb_{10}(PO_4)_6F_2$	23.5	1.185	602.2
$Pb_{10}(PO_4)_6OH_2$	26.7	1.189	603.2
$Pb_{10}(PO_4)_6Cl_2$	17.6	1.208	635.8
$Pb_{10}(VO_4)_6Cl_2$	17.5	1.235	676.5
$Pb_{10}(VO_4)_6I_2$	16.7	1.253	702.4
$Ba_{10}(PO_4)_6F_2$	22.5	1.219	690.3
$Ba_{10}(PO_4)_6Cl_2$	21.0	1.242	700.8
$Ba_{10}(MnO_4)_6Cl_2$	22.3	1.254	736.6
$Ba_{10}(AsO_4)_4(SO_4)_2S$	16.2	1.259	742.4

† Calculated using effective ionic radii of Shannon (1976).

structure type (Engel & Fischer, 1985). It is possible that trivalent bismuth-rich apatites may also exploit the space-filling properties of the lone pairs (Huang & Sleight, 1993; Buvaneswari & Varadaraju, 2000); however, this is yet to be demonstrated. The calculations of Le Bellac *et al.* (1995) have proved useful in locating electron lone pairs in complex oxides, such as $Pb_3P_2O_8$ and $Bi_2Sr_2CaCu_2O_8$, and, if applied to plumbous apatites, would underpin a quantitative discussion on this point.

It has been demonstrated that metals may also be incorporated into the $2a/2b$ sites. Carillo-Cabrera & von Schnering (1999) successfully synthesized $Sr_5(VO_4)_3(Cu_{0.896}O_{0.95})$, in which $(Cu-O)$ strings filled the X positions. While presently the only example of this type, it is not inconceivable that other linearly bonded cation–oxygen strings (*e.g.* $Pd^{1+}-O$, $Ag^{1+}-O$, $Hg^{2+}-O$) might also be prepared, provided larger A (*e.g.* Ba^{2+}) and B (*e.g.* Mn^{5+}) ions are available to sufficiently dilate the unit cell.

3.3. Polysomatism

All $[A(1)_2][A(2)_3](BO_4)_3X$ apatites of whatever symmetry regularly fill every other BO_4 tetrahedral interstice in corner-connected strings along [001] (Fig. 10). Alternative filling schemes are of course possible, such that the same overall occupancy is maintained while producing crystallographically distinct polysomes. Alternate filling has been observed in two minerals – nasonite and ganomalite (Engel, 1972). Nasonite, which has the ideal formula $Pb_6Ca_4(Si_2O_7)_3Cl_2$, was determined by Giuseppetti *et al.* (1971) to have $P6_3/m$ symmetry with consecutive sites filled as Si_2O_7 units. Brès *et al.* (1987) used high-resolution electron microscopy to demonstrate that the situation is more complex, as on the unit-cell scale $P6_3/m$ symmetry is broken. For the intermediate mineral ganomalite (Carlson *et al.*, 1997) Si_2O_7 units alternate with SiO_4 tetrahedra to give an ideal formula $Pb_6Ca_{3.33}Mn_{0.67}(SiO_4)_2(Si_2O_7)_2$ and a structure that conforms to $P\bar{6}$ symmetry. In this compound Pb cations (IR 1.29 Å) are distributed into the larger $6l$, $3k$ sites as expected; the Ca (1.12 Å) occupy the $2i$, $2h$, $1c$ metaprisms in an ordered way with a height along (001) of 3.5 Å, while Ca/Mn (average IR 1.04 Å) on $1e$ fill an untwisted prism of height 3.07 Å (Fig. 11). Intergrowth between apatite layers that have different heights and twist angles is yet another mechanism for accommodating cations of substantially different ionic radii. A more rigorous determination of natural nasonite will probably reveal similar detail. In addition, the synthetic analogue of ganomalite $Pb_5(GeO_4)(Ge_2O_7)$ has been studied extensively because of its ferroelectric properties (Newnham *et al.*, 1973; Iwata, 1977). Stemmermann (1992) synthesized the longer-period $Pb_{40}(Si_2O_7)_6(Si_4O_{13})_3$ with $c = 28.7$ Å. All the members so far reported for the apatite–nasonite family are lead-rich with the role of lone-pair stabilization yet to be fully investigated. Note
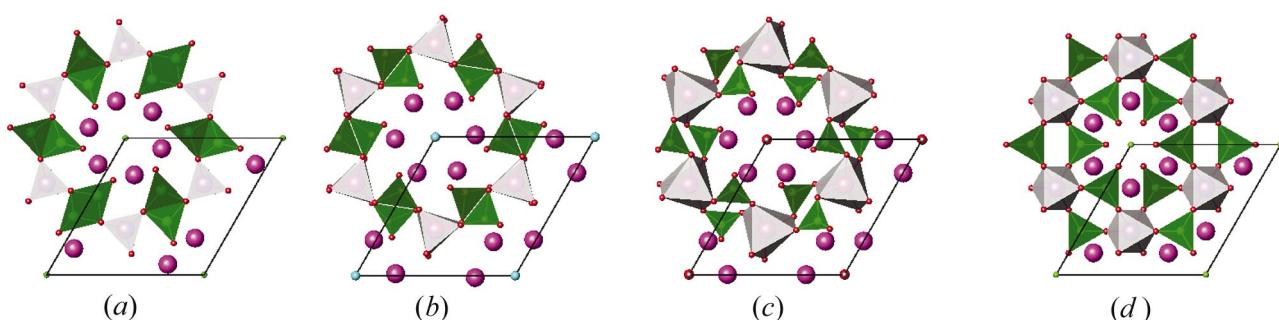
Figure 8
The preferred topological representation of four apatites; both the $A(1)O_6$ trigonal prisms/metaprisms and the BO_4 tetrahedra are emphasized. The idealized structural endmembers are emphasized in (*a*) model I with $\varphi = 0°$ and (*d*) model III with $\varphi = 60°$. The intermediate structures shown are for (*b*) hedyphane $Ca_4Pb_6(AsO_4)_6Cl_2$ with $\varphi = 5.2°$ and (*c*) $Pb_{10}(PO_4)_6(OH)_2$ with $\varphi = 26.7°$.

that stoichiometric adjustments are required in order to generate these tetrahedrally ordered apatite superstructures, and therefore these compounds are described as part of a polysomatic, rather than polytypic, series (Table 6).

4. Apatites with BO_5 and BO_3 polyhedra

The description of apatite as an anion-stuffed alloy proves especially compelling when the scope of the apatite family is broadened to include the less common $[A(1)_2][A(2)_3](BO_5)_3X$ and $[A(1)_2][A(2)_3](BO_3)_3X$ compounds (Table 7). In these cases a greater or lesser number of M_4, M_3 and M_2 metal interstices are filled with oxygen while the distinctive metal arrangement of the $D8_8$ aristotype is maintained.

Finnemanite $Pb_5(AsO_3)_4Cl$ (Effenberger & Pertlik, 1977) is a reduced form of mimetite $Pb_5(AsO_4)_4Cl$ (Dai et al., 1991). Both compounds adopt $P6_3/m$ symmetry with the former missing one $6h$ oxygen to compensate for the substitution of $As^{5+} \leftrightarrow As^{3+}$. In finnemanite the BO_4 tetrahedron is completely replaced by BO_3 with the arsenic lying above the triangular oxygen plane (Fig. 12a). To date, this is the only reported example of a completely ordered $[A(1)_2][A(2)_3](BO_3)_3X$ apatite. However, partial substitutions of BO_3 for BO_4 are known. In biologically important carbonated hydroxyapatite, recent studies confirm that partial replacement of $PO_4^{3-} \leftrightarrow CO_3^{3-}$, which is similar to $AsO_4^{3-} \leftrightarrow AsO_3^{3-}$, occur. However, ordering is incomplete, as either of the two possible O_3 triangular faces that lie parallel to [001] of the BO_4 tetrahedron can be used to accommodate the carbonate unit (Ivanova et al., 2001). It must also be feasible to introduce boron in a s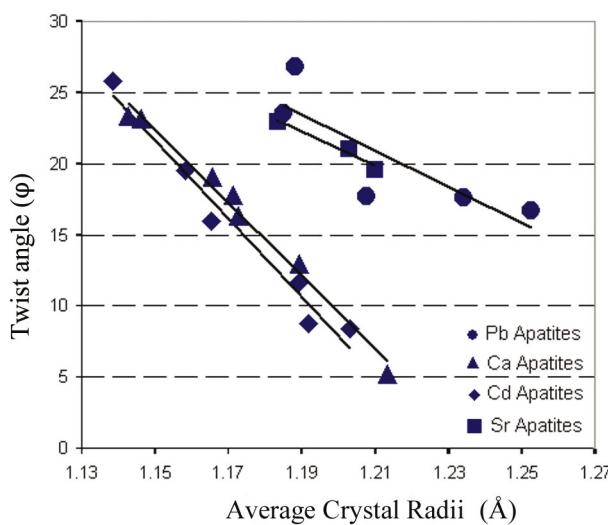imilar way. Ito et al. (1988) have reported the existence of $[Ca_{9.93}(P_{5.84}B_{0.16})_4]_6(B_{0.067}O_{1.79})$; however, whether a preference is shown by BO_3 to occupy particular face(s) of the O_4 tetrahedron has not been resolved.

A number of ruthenates and osmates have been described (Schriewer & Jeitschko, 1993) whose structures are also derived from the $D8_8$ alloy (O'Keeffe & Hyde, 1985). In this case, four of the five O atoms of the BO_5 square pyramid are in OM_4 tetrahedra, while the last is in linear OM_2 coordination (Fig. 12c). In $[A(1)_2][A(2)_3](BO_5)_3X$ compounds the BO_5 pyramids have a 'sense of direction' in that their apical O atoms can lie up or down along [001], and indeed examples of both types have been discovered (Schriewer & Jeitschko, 1993; Plaisier et al., 1995). In $Ba_5(ReO_5)_4Cl$, with $P6_3cm$ symmetry, all of the ReO_5 pyramids' apices are unidirectional, whereas in $Pnma$ $Sr_5(ReO_5)_4Cl$ one-third of the ReO_5 strings adopt antiparallel orientations (Fig. 13).

Finally, an interesting example of an apatite-related structure is $Sr_5(BO_3)_3Br$ (Alekel & Keszler, 1992). It can be regarded as a condensed apatite phase, even though the stoichiometry is outwardly similar to that of finnemanite.[2] In all other structures that we discuss, the AO_6 metaprisms are connected exclusively through $BO_3/BO_4/BO_5$ polyhedra, whereas in $Sr_5(BO_3)_3Br$ some SrO_6 prism columns share an edge with their neighbour – a comparison of Figs. 7(a) and 14 makes the relationship clear. Following the proposition of Moore & Araki (1977) it is possible to isolate $Sr_4(BO_3)_{12}$ as the stable unit of this structure. This unit is analogous to $Ca_4(PO_4)_{12}$ columns, which through rotational operations can generate significant segments of the structures of hydroxyapatite, octacalcium phosphate and samuelsonite. However,
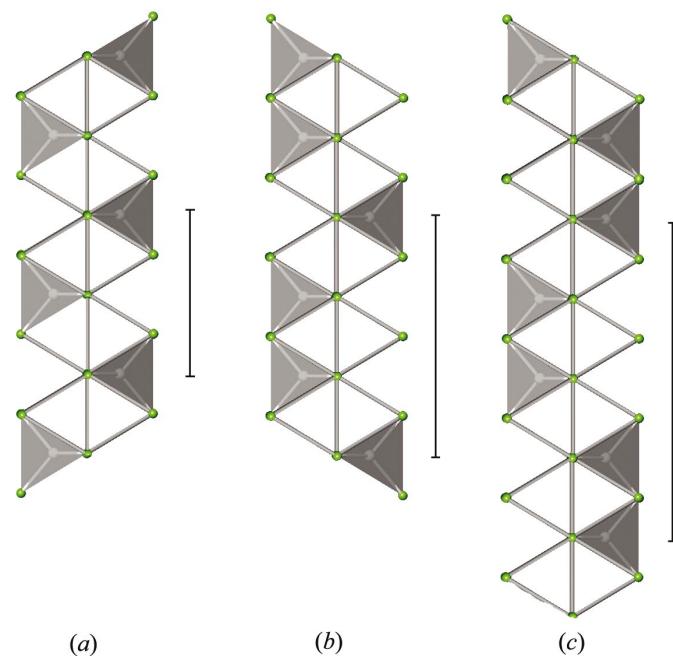
Figure 9
Relationship between twist angle (φ) and average crystal radius for several $[A(1)_2][A(2)_3](BO_4)_3X$, $P6_3/m$, apatites in which the A cation is fixed and only B and X vary. For the Ca- and Cd-apatites there is very nearly a linear relationship. This also holds true for Sr-apatites although only three examples were included. While the general trend is also true for the Pb-apatites, the relationship is not so direct.

Figure 10
Tetrahedral strings and c-axis repetition in (a) apatite, c_{ap}, (b) ganomalite, $\sim 1.33 c_{ap}$, and (c) nasonite, $\sim 2 c_{ap}$.

---

[2] Compositionally similar $Mg_5(BO_3)_3F$ is unrelated to finnemanite and is a leucophoenicite-type mineral (White & Hyde, 1983).

Table 6
Polysomatic apatites.

Mineral name	Space group	Composition	Unit-cell parameters (Å)	Reference
	$P\bar{6}$	$Pb_5(GeO_4)(Ge_2O_7)$	$a = 10.260$, $c = 10.696$	Iwata (1977)
Ganomalite	$P\bar{6}$	$Pb_9Ca_5Mn(Si_2O_7)_3(SiO_4)_3$	$a = 9.850$ (50), $c = 10.130$ (50)	Carlson *et al.* (1997)
	$P\bar{6}$	$Pb_9Ca_6(Si_2O_7)_3(SiO_4)_3$	$a = 9.875$, $c = 10.176$	Stemmermann (1992)
	$P\bar{6}$	$Pb_{12}Ca_3(Si_2O_7)_3(SiO_4)_3$	$a = 9.880$, $c = 10.210$	Stemmermann (1992)
	$P\bar{6}$ (?)	$Pb_3Ca_2(Si_2O_7)(SiO_4)$	$a = 9.879$ (1), $c = 10.178$ (1)	Engel (1972)
	$P\bar{6}$ (?)	$Pb_3BiNa(Si_2O_7)(SiO_4)$	$a = 9.876$ (1), $c = 10.175$ (1)	Engel (1972)
	$P\bar{6}$ (?)	$Pb_3Cd_2(Si_2O_7)(SiO_4)$	$a = 9.810$ (4), $c = 10.124$ (4)	Engel (1972)
	$P\text{-}6$ (?)	$Pb_3Ca_2(Ge_2O_7)(GeO_4)$	$a = 10.104$ (1), $c = 10.379$ (1)	Engel (1972)
	$P\bar{6}$ (?)	$Pb_3BiNa(Ge_2O_7)(GeO_4)$	$a = 10.084$ (1), $c = 10.398$ (1)	Engel (1972)
	$P\bar{6}$	$Pb_6Ca_4(Si_2O_7)_3Cl_2$	$a = 10.074$, $c = 13.234$	Stemmermann (1992)
Nasonite	$P\bar{6}$ (?)	$Pb_9Ca_4(Si_2O_7)_3$	$a = 10.080$, $c = 13.270$	Giuseppetti *et al.* (1971)
	Monoclinic (?)	$Pb_{40}(Si_2O_7)_6(Si_4O_{13})_3$	$a = 17.075$, $b = 9.844$, $c = 26.678$, $\beta = 90.09°$	Stemmermann (1992)

as yet the range of available compounds is insufficient to test this hypothesis.

5. Discussion and conclusions

In summarizing the crystallographic data for the materials $[A(1)_2][A(2)_3](BO_4)_3X$, $[A(1)_2][A(2)_3](BO_5)_3X$ and $[A(1)_2][A(2)_3](BO_3)_3X$, their description as 'apatite' or 'apatite-related' can be replaced by a formal description as anion-stuffed hettotypes of the $D8_8$ aristotype. From this perspective, all are members of the apatite structural family, in the same way that even rather complex perovskites (such as giant magnetoresistance $CaCu_3Mn_4O_{12}$ and superconducting $YBa_2Cu_3O_{7-\delta}$) possess similar genealogy. This proposition has been most fully articulated by O'Keeffe & Hyde (1985) but has also been recognized by Wondratschek *et al.* (1964) and more recently Schriewer & Jeitschko (1993) and Vegas & Jansen (2002). When formalized, this approach leads to a hierarchical tree of possible symmetries, which is increasingly pertinent as the structures of more apatites become available. While $P6_3/m$ is the most common symmetry of $[A(1)_2][A(2)_3](BO_4)_3X$ apatites, it is by no means dominant. With increasing chemical complexity, the lower symmetries $P6_3$, $P\bar{3}$, $P\bar{6}$, $P2_1/m$ and $P2_1$ are required in order to accommodate cation ordering, and it may be expected that additional lower-symmetry varieties will be recognized. Huang & Sleight (1993) have noted that many $P6_3/m$ apatites may actually have lower symmetry, and this prescience is borne out by high-precision redeterminations. The most recent of these is the reinvestigation of cesanite $Na_{6.9}Ca_{3.1}(SO_4)_6(OH)_{1.1}$ by Piotrowski, Kahlenberg, Fischer *et al.* (2002), who through the careful analysis of systematic absences were able to allocate $P\bar{6}$ as the correct symmetry.

The middle branch of the structural tree, the branch that leads from $P6_3/m$, is evidentially the most heavily populated, with only a few representatives reported for the $Cmcm$ and
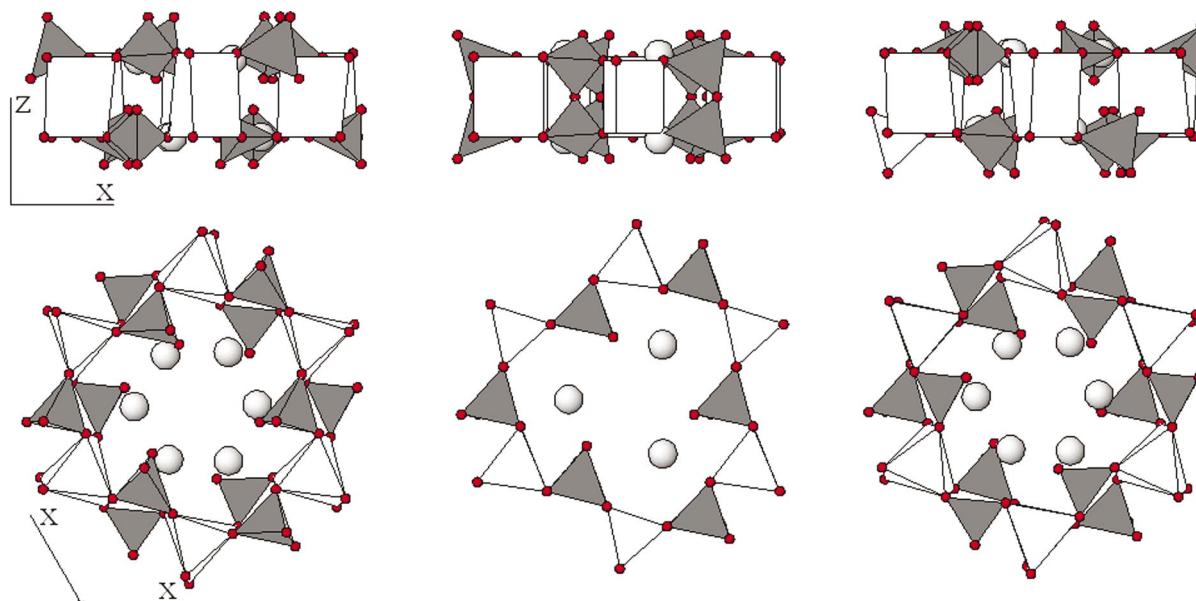

Figure 11
The three apatite layers in ganomalite $Pb_6Ca_{3.33}Mn_{0.67}(SiO_4)_2(Si_2O_7)_2$. The figure demonstrates the intergrowth of layers with different twist angles (φ). Layers 1 and 3 contain trigonal prisms whose triangular faces are of different size and $\varphi = 17.2°$. Layer 2, which contains the Mn atom, has $\varphi = 0°$. In the upper portion of the drawing the connectivity of the SiO_4 tetrahedra are emphasized; the Si_2O_7 unit occurs in the middle layer.

Table 7
$[A(1)_2][A(2)_3](BO_5)_3X$ and $[A(1)_2][A(2)_3](BO_3)_3X$ apatites.

| Mineral name	Space group	Composition	Unit-cell parameters (Å)	Reference
Finnemanite	$P6_3/m$	$Pb_5(AsO_3)_3Cl$	$a = 10.322\ (7),\ c = 7.054\ (6)$	Effenberger & Pertlik (1977)
	$C222_1$	$Sr_5(BO_3)_3Br$	$a = 10.002\ (2),\ b = 14.197\ (2),\ c = 7.458\ (1)$	Alekel & Keszler (1992)
	$P6_3cm$	$Ba_5(ReO_5)_3NO_4$	$a = 11.054\ (5),\ c = 7.718\ (4)$	Aneas et al. (1983)
	$P6_3cm$	$Ba_5(ReO_5)_3Cl$	$a = 10.926\ (1),\ c = 7.782\ (1)$	Schriewer & Jeitschko (1993); Besse et al. (1979)
	$P6_3cm$	$Ba_5(OsO_5)_3Cl$	$a = 10.928\ (2),\ c = 7.824\ (5)$	Plaisier et al. (1995)
	$Pnma$	$Sr_5(ReO_5)_3Cl$	$a = 7.438\ (1),\ b = 18.434\ (2),\ c = 10.563\ (2)$	Schriewer & Jeitschko (1993)
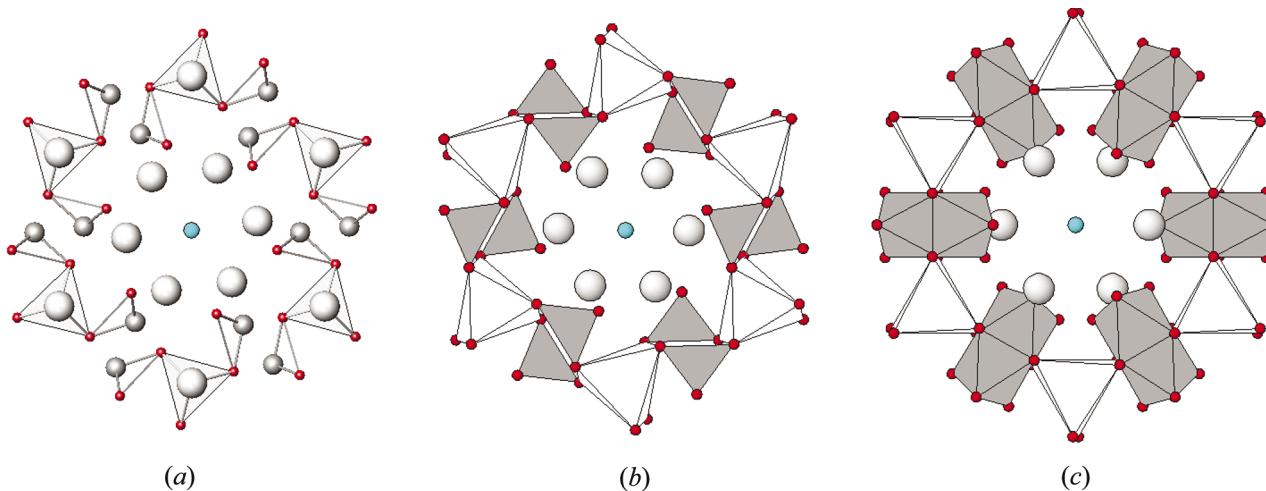
Figure 12
The structures of (a) finnemanite $Pb_5(AsO_3)_4Cl$, (b) mimetite $Pb_5(AsO_4)_4Cl$ and (c) $Ba_5(ReO_5)_4Cl$. The figures show the progressive insertion of oxygen, the conversion of AsO_3 to AsO_4 and the ReO_5 coordination. In finnemanite the Pb(1) ions are drawn as they occupy half-trigonal prisms (with three capping O atoms at a greater distance). Stereochemically active lone-pairs probably play a key role in stabilizing this structure.

$P6_3cm$ branches. However, for the latter, the chemistries studied remain sparse, and it is possible that new representatives with stoichiometry $[A(1)_2][A(2)_3](BO_5)_3X$ will be discovered.

The derivation of apatites from a regular oxygen sublattice also proves valuable, as it includes the BO_4 tetrahedra that are the common recognizable units shown in most structure drawings. These ideas, first used by Povarennykh (1972) and developed by Alberius-Henning, Landa-Canovas et al. (1999), have been extended in this paper to include the $A(1)O_6$ trigonal metaprisms as a key structural unit, along with the BO_4 tetrahedra, in order to portray apatite chemical series. This depiction provides a highly visual and quantitative measure of apatite distortion from a perfect hexagonal anion net. For apatites that contain one species of A cation, the metaprismatic twist angle φ varies linearly over a wide range of compositions and changes inversely with atomic radius. The analysis of φ can be used to rapidly detect structures that fall outside expected bounds or deviate from compositional trends. Naturally, φ is not in itself sufficient to dismiss a structure solution as deficient; however, φ can indicate possible misinterpretation, particularly with respect to symmetry. For apatites that contain mixed and ordered $A(1)$ cations, the interpretation becomes more complex, as the height of the metaprism (along [001]) is also influenced by the

requirement to satisfy $A-O$ bond lengths. In work to be published for $(Ca_{10-x}Pb_x)(VO_4)_6(O,F)_{2-\delta}$, $0 < x < 9$, apatites (Dong & White, 2003), φ has been used as a sensitive probe to detect disequilibrium. Furthermore, microdomains observed directly by HRTEM were only removed after φ stabilized.

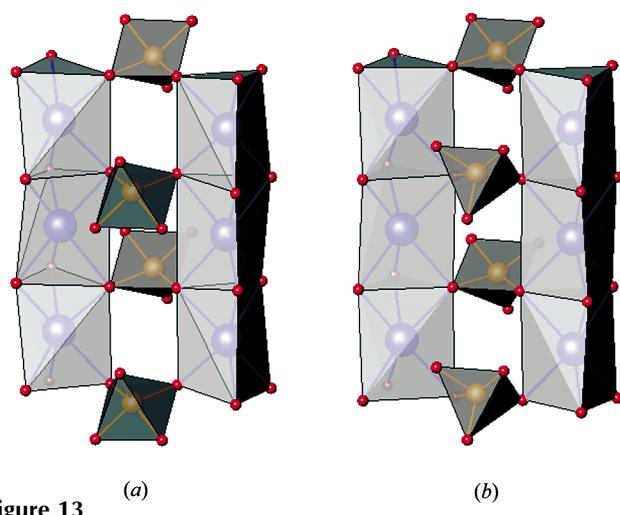**Figure 13**
The arrangement of ReO_5 square pyramids in (a) $Sr_5(ReO_5)_4Cl$, where the directionality is antiparallel between some SrO_6 metaprisms, and (b) $Ba_5(ReO_5)_4Cl$, where the arrangement is always parallel, i.e. with the apical oxygen always pointing the same way.

research papers

The structural relationship between apatite and nasonite is well established (Engel, 1972), and members of this polysomatic series are possibly more prevalent than is currently recognized. Ganomalite $Pb_6Ca_{3.33}Mn_{0.67}(SiO_4)_2(Si_2O_7)_2$ (Carlson *et al.*, 1997) and $Pb_{40}(Si_2O_7)_6(Si_4O_{13})_3$ (Stemmermann, 1992) have been identified as intermediate members of this homologous series. However, the structural principle of ordered filling of tetrahedral sites can give rise to an indefinite number of structures. It is less clear whether lead is a critical component of these structures but all current examples are substantially plumbous. At the atomic level, these structures may be quite complex. In the one instance where single-crystal X-ray diffraction and HRTEM have been undertaken, Brès *et al.* (1987) observed on the same sample a clear discrepancy in crystallographic features, the diffraction results being consistent with well ordered $P6_3/m$, while direct imaging showed microdomains of lower symmetry.

The rich chemistry and structural diversity of apatites provides fertile ground for the synthesis of technology-relevant compounds. Novel materials will continue to be discovered and possibly exploited in such diverse applications as zinc-rich bioactive apatites that accelerate tissue regrowth, mercury-bearing compounds analogous to $Sr_5(VO_4)_3(Cu_{0.896}O_{0.95})$ for polishing industrial wastewaters and catalytic apatites for photovoltaic devices.
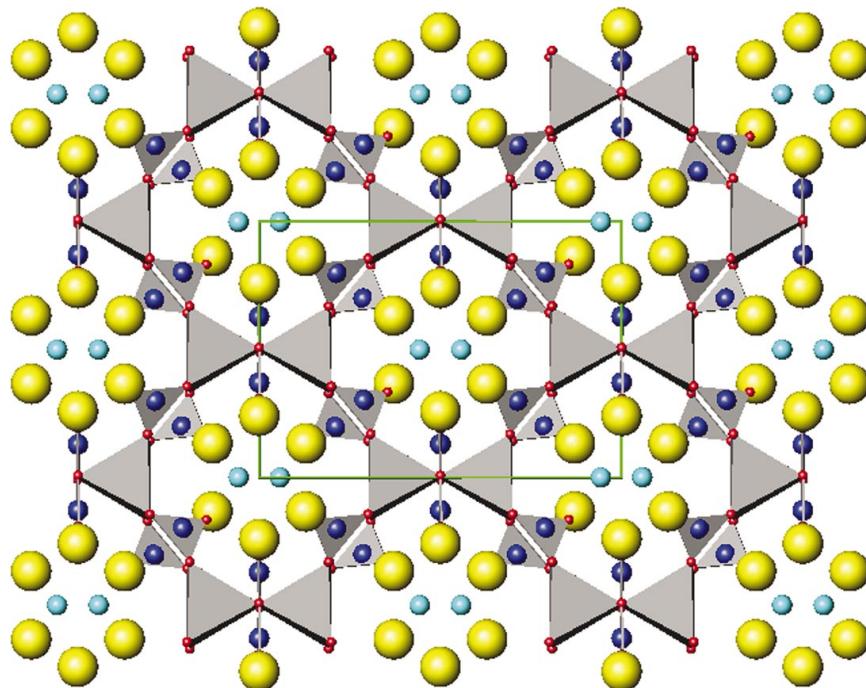
Figure 14
$Sr_5(BO_3)_3Br$ projected on (001). The apatite-like elements are obvious but are condensed such that some SrO_6 trigonal prisms share edges rather than being connected through BO_3 triangles.

References

Alberius-Henning, P., Landa-Canovas, A. R., Larddon, A.-K. & Lidin, S. (1999). *Acta Cryst.* B**55**, 170–176.

Alberius-Henning, P., Lidin, S. & Petrícek, V. (1999). *Acta Cryst.* B**55**, 165–169.

Alekel, T. & Keszler, D. A. (1992). *Acta Cryst.* C**48**, 1382–1386.

Aneas, M., Picard, J. P., Baud, G., Besse, J. P. & Chevalier, R. (1983). *Mater. Chem. Phys.* **8**, 119–123.

Audubert, F., Savariault, J.-M. & Lacout, J.-L. (1999). *Acta Cryst.* C**55**, 271–273.

Barinova, A. V., Bonin, M., Pushcharovskii, D. Yu., Rastsvetaeva, R. K., Schenk, K. & Dimitrova, O. V. (1998). *Kristallografiya*, **43**, 224–227.

Bauer, M. & Klee, W. E. (1993). *Z. Kristallogr.* **206**, 15–24.

Belokoneva, E. L., Troneva, E. A., Dem'yanets, L. N., Duderov, N. G. & Belov, N. V. (1982). *Kristallografiya*, **27**, 793–794.

Besse, J.-P., Baud, G., Levasseur, G. & Chevalier, R. (1979). *Acta Cryst.* B**35**, 1756–1759.

Bondareva, O. S. & Malinovskii, Yu. A. (1986). *Kristallografiya*, **31**, 233–236.

Brès, E. F., Waddington, W. G., Hutchison, J. L., Cohen, S., Mayer, I. & Voegel, J.-C. (1987). *Acta Cryst.* B**43**, 171–174.

Brown, P. W. & Constantz, B. (1994). Editors. *Hydroxyapatite and Related Materials.* Boca Raton: CRC Press.

Bruecker, S., Liusvardi, G., Menabue, L. & Saladini, M. (1995). *Inorg. Chim. Acta*, **236**, 209–212.

Buvaneswari, G. & Varadaraju, U. V. (2000). *J. Solid State Chem.* **149**, 133–136.

Calos, N. J. & Kennard, C. H. L. (1990). *Z. Kristallogr.* **191**, 125–129.

Calvo, C., Faggiani, R. & Krishnamachari, N. (1982). *Acta Cryst.* B**31**, 188–192.

Carlson, S., Norrestam, R., Holtstam, D. & Spengler, R. (1997). *Z. Kristallogr.* **212**, 208–212.

Carrillo-Cabrera, W. & von Schnering, H. G. (1999). *Z. Anorg. Allg. Chem.* **625**, 183–185.

Christy, A. G., Alberius-Henning, P. & Lidin, S. A. (2001). *J. Solid State Chem.* **156**, 88–100.

Cockbain, A. G. (1968). *Mineral. Mag.* **37**, 654–660.

Corker, D. L., Chai, B. H. T., Nicholls, J. & Loutts, G. B. (1995). *Acta Cryst.* C**51**, 549–551.

Dai, Y.-S. & Hughes, J. M. (1989). *Can. Mineral.* **27**, 189–192.

Dai, Y.-S., Hughes, J. M. & Moore, P. B. (1991). *Can. Mineral.* **29**, 369–376.

Dardenne, K., Vivien, D. & Huguenin, D. (1999). *J. Solid State Chem.* **146**, 464–472.

Donaldson, J. D. & Grimes, S. M. (1984). *J. Chem Soc. Dalton Trans.* pp. 1301–1305.

Dong, Z. L. & White, T. J. (2003). In preparation.

Effenberger, H. & Pertlik, F. (1977). *Tschermaks Mineral. Petrogr. Mitt.* **26**, 95–107.

Elliot, J. C. (1994). *Structure and Chemistry of the Apatites and Other Calcium Orthophosphates.* Amsterdam: Elsevier.

Elliot, J. C., Dykes, E. & Mackie, P. E. (1981). *Acta Cryst.* B**37**, 435–438.

Elliot, J. C., Mackie, P. E. & Young, R. A. (1973). *Science*, **180**, 1055–1057.

Engel, G. (1972). *Naturwissenschaften*, **59**, 121–122.

Engel, G. & Deppisch, B. (1988). *Z. Anorg. Allg. Chem.* **562**, 131–140.

Engel, G. & Fischer, U. (1985). *Z. Kristallogr.* **173**, 101–112.

Engel, G. & Fischer, U. (1990). *J. Less-Common Metals*, **158**, 123–130.

Engel, G., Pretzsch, J., Gramlich, V. & Baur, W. H. (1975). *Acta Cryst.* B**31**, 1854–1860.

Gaude, J., L'Haridon, P., Hamon, C., Marchand, R. & Laurent, Y. (1975). *Bull. Soc. Mineral. Crist. Fr.* **98**, 214–217.

Genkina, E. A., Malinovskii, Yu. A. & Khomyakov, A. P. (1991). *Kristallografia*, **36**, 39–43.

Giuseppetti, G., Rossi, G. & Tadini, C. (1971). *Am. Mineral.* **56**, 1174–1179.

Gunawardane, R. P., Howie, R. A. & Glasser, F. P. (1982). *Acta Cryst.* B**38**, 1564–1566.

Hashimoto, H. & Matsumoto, T. (1998). *Z. Kristallogr.* **213**, 585–590.

Hata, M. & Marumo, F. (1983). *Mineral. J.* (*Jpn*), **11**, 317–330.

Hata, M., Marumo, F. & Iwai, S. I. (1979). *Acta Cryst.* B**35**, 2382–2384.

Hata, M., Marumo, F. & Iwai, S. I. (1980). *Acta Cryst.* B**36**, 2128–2130.

Hata, M, Okada, K., Iwai, S. I., Akao, M. & Aoki, H. (1978). *Acta Cryst.* B**34**, 3062–3064.

Hendricks, S. B., Jefferson, M. E. & Mosley, V. M. (1932). *Z. Kristallogr. Kristallogeom. Kristallphys. Kristallchem.* **81**, 352–369.

Howie, R. A., Moser, W., Starks, R. G., Woodhams, F. W. D. & Parker, W. (1973). *J. Chem. Soc. Dalton Trans.* pp. 1478–1484.

Huang, J. & Sleight, A. W. (1993). *J. Solid State Chem.* **104**, 52–58.

Hughes, J. M., Cameron, M. & Crowley, K. D. (1989). *Am. Mineral.* **74**, 870–876.

Hughes, J. M. & Drexler, J. W. (1991). *N. Jahrb. Mineral. Monatsh.* pp. 327–336.

Hughes, J. M., Mariano, A. N. & Drexler, W. (1992). *N. Jahrb. Mineral. Monatsh.* pp. 311–319.

Ikoma, T., Yamazaki, A., Nakamura, S. & Akoa, M. (1999). *J. Solid State Chem.* **144**, 272–276.

Ito, A., Akao, M., Miura, N., Otsuka, R. & Tsutsumi, S. (1988). *Nippon Seramikkusu Kyokai Gakujutsu Ronbunshi*, **96**, 305–309. [Abstracted from ICSD, Collection Code 68336, Gmelion Institute, Fiz Karlsruhe.]

Ivanov, A., Simonov, M. A. & Belov, N. (1976). *Zh. Struk. Khim.* **17**, 375–378.

Ivanov, S. A. (1990). *J. Struct. Chem.* **31**, 80–84.

Ivanov, S. A. & Zavodnik, V. E. (1989). *Sov. Phys. Crystallogr.* **34**, 493–496.

Ivanova, T. I., Frank-Kamenetskaya, O. V., Kol'tsov, A. B. & Ugolkov, V. L. (2001). *J. Solid State Chem.* **160**, 340–349.

Iwata, Y. (1977). *J. Phys. Soc. Jpn*, **43**, 961–967.

Kabalov, Yu. K., Sokolova, E. V. & Pekov, I. V. (1997). *Dokl. Akad. Nauk*, **355**, 182–185.

Kalsbeek, N., Larsen, S. & Ronsbo, J. G. (1990). *Z. Kristallgr.* **191**, 249–263.

Kim, J. Y., Fenton, R. R., Hunter, B. A. & Kennedy, B. J. (2000). *Aust. J. Chem.* **53**, 679–686.

Kim, J. Y., Hunter, B. A., Fenton, R. R. & Kennedy, B. J. (1997). *Aust. J. Chem.* **50**, 1061–1065.

Klevtsova, P. F. (1964). *Zh. Strukt. Khim.* **5**, 318–320.

Klevtsova, P. F. & Borisov, S. V. (1964). *Zh. Strukt. Khim.* **5**, 151–153.

Kluever, E. & Mueller-Buschbaum, Hk. (1995). *Z. Naturforsch. Teil B*, **50**, 61–65.

Le Bellac, D., Kiat, J. M. & Garnier, P. (1995). *J. Solid State Chem.* **114**, 459–468.

Lefkowitz, I., Łukaszewicz, K. & Megaw, H. D. (1966). *Acta Cryst.* **20**, 670–683.

McConnell, D. (1973). *Apatite, Its Crystal Chemistry, Mineralogy, Utilization, and Geologic and Biologic Occurrences.* Wein: Springer-Verlag.

Mackie, P. E., Elliot, J. C. & Young, R. A. (1972). *Acta Cryst.* B**28**, 1840–1848.

Malinovskii, Yu. A., Genekina, E. A. & Dimitrova, O. V. (1990). *Kristallografiya*, **35**, 328–331.

Malinovskii, Yu. A., Pobedimskaya, E. A. & Belov, N. V. (1975). *Kristallografiya*, **20**, 644–646.

Mathew, M., Brown, W. E., Austin, M. & Negas, T. (1980). *J. Solid State Chem.* **35**, 69–76.

Mathew, M., Mayer, I., Dickens, B. & Schroeder, L. W. (1979). *J. Solid State Chem.* **28**, 79–95.

Mattausch, H. J. & Mueller-Buschbaum, Hk. (1973). *Z. Anorg. Allg. Chem.* **400**, 1–9.

Maunaye, M., Hamon, C., L'Haridob, P. & Laurent, Y. (1976). *Bull. Soc. Mineral. Crist. Fr.* **99**, 203–205.

Mazza, D., Tribaudino, M., Delmastro, A. & Lebech, B. (2000). *J. Solid State Chem.* **155**, 389–393.

Megaw, H. D. (1973). *Crystal Structures: A Working Approach*, p. 216. Philadelphia: W. B. Saunders.

Moore, P. B. & Araki, T. (1977). *Am. Mineral.* **62**, 229–245.

Mueller-Buschbaum, Hk. & Sander, K. (1978). *Z. Naturforsch. Teil B*, **33**, 708–710.

Nadezhina, T. N., Pushcharovskii, D. Yu. & Khomyakov, A. P. (1987). *Mineral. Zh.* **9**, 45–48.

Naray-Szabo, S. (1930). *Z. Kristallogr. Kristallgeom. Kristallphys. Kristallchem.* **75**, 387–398.

Newnham, R. E., Wolfe, R. W. & Darlington, C. N. W. (1973). *J. Solid State Chem.* **6**, 378–383.

Noe, D. C., Hughes, J. M., Marino, A. N., Drexler, J. W. & Kato, A. (1993). *Z. Kristallogr.* **206**, 233–246.

Nötzold, D. & Wulff, H. (1998). *Powder Diffr.* **13**, 70–73.

Nötzold, D., Wulff, H. & Herzog, G. (1994). *J. Alloys Compd.* **215**, 281–288.

Nriagu, O. & Moore, P. B. (1984). Editors. *Phosphate Minerals.* Berlin: Springer-Verlag.

Nyman, H. & Andersson, S. (1979). *Acta Cryst.* A**35**, 580–583.

O'Keeffe, M. & Hyde, B. G. (1985). *Struct. Bonding*, **61**, 77–144.

O'Keeffe, M. & Hyde, B. G. (1996). *Crystal Structures I. Patterns and Symmetry.* Washington: Mineralogical Society of America.

Organova, N. I., Rastsvetaeva, R. K., Kuz'mina, O. V., Arapova, G. A., Litsarev, M. A. & Fin'ko, V. I. (1994). *Kristallografiya*, **39**, 278–282.

Piotrowski, A., Kahlenberg, V. & Fischer, R. X. (2002). *J. Solid State Chem.* **163**, 398–405.

Piotrowski, A., Kahlenberg, V., Fischer, R. X., Lee, Y. & Parize, J. B. (2002). *Am. Mineral.* **87**, 715–720.

Plaisier, J. R., de Graaff, R. A. G. & Ijdo, D. J. W. (1995). *Mater. Res. Bull.* **30**, 1249–1252.

Povarennykh, A. S. (1972). *Crystal Chemical Classification of Minerals*, pp. 541–542. New York/London: Plenum Press.

Pushcharovskii, D. Y., Dorokhova, G. I., Pobedimskaya, E. A. & Belov, N. V. (1978). *Dokl. Akad. Nauk*, **242**, 835–838.

Pushcharovskii, D. Y., Nadezhina, T. N. & Khomyakov, A. P. (1987). *Kristallografiya*, **37**, 891–895.

Reinen, D., Lachwa, H. & Allmann, R. (1986). *Z. Anorg. Allg. Chem.* **542**, 71–88.

Rouse, R. C., Dunn, P. J. & Peacor, D. R. (1984). *Am. Mineral.* **89**, 920–927.

Schiff-Francois, A., Savelsberg, G. & Schaefer, H. (1979). *Z. Naturforsch. Teil B*, **34**, 764–765.

Schneider, W. (1967). *N. Jahrb. Mineral. Monatash.* pp. 284–289.

Schneider, W. (1969). *N. Jahrb. Mineral. Monatsh.* pp. 58–64.

Schriewer, M. S. & Jeitschko, W. (1993). *J. Solid State Chem.* **107**, 1–11.

Shannon, R. D. (1976). *Acta Cryst.* A**32**, 751–767.

Sirotinkin, S. P., Oboznenko, Yu. V. & Nevskii, N. N. (1989). *Russ. J. Inorg. Chem.* **34**, 1716–1718.

Stemmermann, P. (1992). PhD thesis, Naturwissenschaftlichen Fakultaten, Freidrich-Alexander-Universitat Erlangen-Nurnberg, Germany.

Sudarsanan, K. (1980). *Acta Cryst.* B**36**, 1636–1639.

Sudarsanan, K., Mackie, P. E. & Young, R. A. (1972). *Mater. Res. Bull.* **7**, 1331–1338.

Sudarsanan, K. & Young, R. A. (1972). *Acta Cryst.* B**28**, 3668–3670.

Sudarsanan, K., Young, R. A. & Donnay, J. D. H. (1973). *Acta Cryst.* B**29**, 808–814.

Sudarsanan, K., Young, R. A. & Wilson, A. J. C. (1977). *Acta Cryst.* B**33**, 3136–3142.

Sutich, P. R., Taitai, A., Lacout, J. L. & Young, R. A. (1986). *J. Solid State Chem.* **63**, 267–277.

Takahashi, M., Uematsu, K., Ye, Z.-G. & Sato, M. (1998). *J. Solid State Chem.* **139**, 304–309.

Toumi, M., Smiri-Dogguy, L. & Bulou, A. (2000). *J. Solid State Chem.* **149**, 308–313.

Vegas, A. & Jansen, M. (2002). *Acta Cryst.* B**58**, 38–51.

Vegas, A., Romero, A. & Martínez-Ripoll, M. (1991). *Acta Cryst.* B**47**, 17–23.

Wardojo, T. A. & Hwu, S-J. (1996). *Acta Cryst.* C**52**, 2959–2960.

White, T. J. & Hyde, B. G. (1983). *Acta Cryst.* B**39**, 10–17.

Wilhelmi, K. A. & Jonsson, O. (1965). *Acta Chem. Scand.* **19**, 177–184.

Wilson, A. J. C., Sudarsanan, K. & Young, R. A. (1977). *Acta Cryst.* B**33**, 3142–3154.

Wondratschek, H. (1963). *N. Jahrb. Miner. Abh.* **99**, 113–160.

Wondratschek, H., Merker, L. & Schubert, K (1964). *Z. Kristallogr.* **120**, 393–395.

Wyckoff, R. W. G. (1965). *Crystal Structures*, Vol. 3, *Inorganic Compounds $R_x(MX_4)y$, $R_x(M_nX_p)_y$, Hydrates and Ammoniates*, pp. 228–234. New York: John Wiley and Sons.